Acta Chemica Scandinavica A 39 (1985) 143–151

Magnetic and Structural Properties of Transition Metal Substituted MnP. V. $Mn_{1-t}Cr_tP$ ($0.00 \leqq t \leqq 0.40$)

HELMER FJELLVÅG,[a] ARNE KJEKSHUS[a] and ARNE F. ANDRESEN[b]

[a] Kjemisk Institutt, Universitetet i Oslo, Blindern, Oslo 3, Norway and [b] Institutt for Energiteknikk, Kjeller, Norway

$Mn_{1-t}Cr_tP$ is studied for $0.00 \leqq t \leqq 0.40$ by X-ray and neutron diffraction and magnetic susceptibility measurements at temperatures between 10 and 1000 K. $Mn_{1-t}Cr_tP$ takes the MnP type structure in para- (P), ferro- (F) or helimagnetic (H_c) states under these conditions. The revised magnetic phase diagram for $Mn_{1-t}Cr_tP$ includes a magnetic two phase region ($\sim 0.02 < t < \sim 0.11$) between the H_c and F phases, leaving only a narrow ternary range ($0.00 \leqq t \leqq \sim 0.02$) for the H_c phase. The results are discussed in relation to other information on $Mn_{1-t}Cr_tP$ and related phases.

The magnetic phase diagram for the MnP–CrP system[1,2] is special among the pseudo-binary $Mn_{1-t}T_tP$ (T=transition metal) solid solutions in that the ferromagnetic (F) phase[2–9] for T=Cr covers wider ranges of composition and temperature than for other transition metals. The existence range of the F phase for $Mn_{1-t}Cr_tP$ extends to $t \approx 0.5$ whereas the helimagnetic (H_c) phase is reported to cease at $t \approx 0.1$.[1,2] The MnP–CrP[1,2] system shows close correspondence to MnP–NiP[7] and some resemblance to MnP–CoP,[2,6] but differs from MnP–VP[2,8] and MnP–FeP.[1,2,9] For the two latter systems the P (paramagnetic), F and H_c phases meet in triple points.

The purpose of the present communication, which forms a continuation of the series of papers[2,6–9] on $Mn_{1-t}T_tP$ phases, is to report crystallographic and magnetic structure data on $Mn_{1-t}Cr_tP$ for $0.00 \leqq t \leqq 0.40$. Brief accounts of the findings are earlier published in Refs. 2,10.

EXPERIMENTAL

Samples of MnP and CrP were made as described in Refs. 6,10. The purities of the elements used as starting materials are given in Ref. 2. Ternary $Mn_{1-t}Cr_tP$ samples were prepared by heating appropriate mixtures of MnP and CrP in evacuated, sealed silica tubes at 1000 °C for two periods of 5 d, interrupted by slow cooling to room temperature and intermediate crushing. Finally, the samples were cooled to room temperature over 1 d.

Details concerning the X-ray and neutron diffraction and magnetic susceptibility measurements are given in Ref. 5. The nuclear neutron scattering lengths (in 10^{-12} cm) $b_{Cr}=0.352$, $b_{Mn}=-0.37$ and $b_P=0.51$ were taken from Ref. 11, and the magnetic form factor for Mn^{2+} from Ref. 12.

0302-4377/85 $2.50

Table 1. Unit cell dimensions and positional parameters with standard deviations for $Mn_{1-t}Cr_tP$ as derived by Rietveld analysis of powder neutron diffraction data. Space group *Pnma*; Mn/Cr in 4*c* and P in 4*c*. (Nuclear R_n-factors ranging between 0.02 and 0.05; magnetic R_m-factors ranging between 0.03 and 0.07; profile R_p-factors ranging between 0.06 and 0.12; 20–25 nuclear reflections.)

t	T(K)	*a*(pm)	*b*(pm)	*c*(pm)	x_T	z_T	x_P	z_P
0.05	293	525.72(8)	316.57(4)	591.62(8)	0.0052(14)	0.1956(14)	0.1868(8)	0.5699(7)
	60	524.65(3)	317.70(2)	590.94(4)	0.0062(10)	0.1971(10)	0.1878(8)	0.5698(7)
	10	524.68(3)	317.67(2)	590.95(4)	0.0069(11)	0.1970(11)	0.1879(18)	0.5696(8)
0.10	293	526.94(9)	316.50(6)	593.38(9)	0.0064(11)	0.1940(12)	0.1887(6)	0.5665(6)
	60	525.21(4)	317.14(3)	591.58(5)	0.0056(15)	0.1953(12)	0.1876(9)	0.5688(7)
	10	525.20(5)	317.09(3)	591.69(6)	0.0081(20)	0.1979(14)	0.1878(12)	0.5678(8)
0.20	293	528.32(8)	315.04(4)	594.93(8)	0.0063(24)	0.1962(24)	0.1888(10)	0.5668(8)
	60	526.75(6)	315.52(3)	593.44(7)	0.0090(21)	0.1974(16)	0.1890(9)	0.5671(8)
	10	526.65(5)	315.60(3)	592.40(6)	0.0085(18)	0.1971(13)	0.1888(8)	0.5676(7)
0.30	293	530.27(7)	314.15(3)	597.16(7)	0.0090(32)	0.1979(32)	0.1885(9)	0.5661(8)
	10	527.90(7)	313.33(4)	594.56(8)	−0.0010(35)	0.2004(29)	0.1867(11)	0.5681(11)
0.40	293	530.87(6)	312.71(3)	597.15(6)	0.0045(51)	0.1974(40)	0.1886(8)	0.5668(6)
	10	529.35(7)	311.95(6)	596.01(6)	0.0028(32)	0.1978(41)	0.1879(9)	0.5676(7)

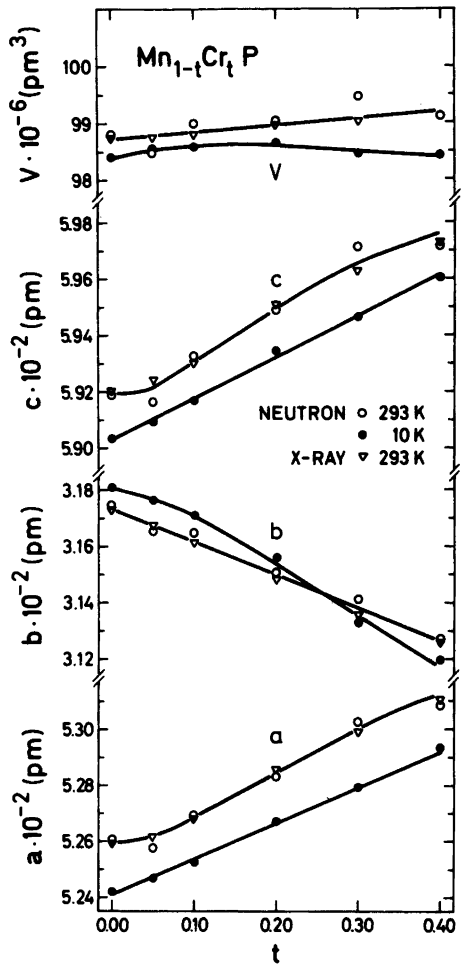

Fig. 1. Unit cell dimensions of $Mn_{1-t}Cr_tP$ *versus* t ($0.00 \leqq t \leqq 0.40$) at 10 and 293 K. Legends to symbols are given on the illustration. *Calculated* error limits do not exceed twice the size of symbols. (1 Å=10^2 pm.)

RESULTS AND DISCUSSION

(i) *Atomic arrangement.* As shown by Selte *et al.*[10] $Mn_{1-t}Cr_tP$ exhibits complete solid solubility for variously heated, quenched and slowly cooled samples. The present results are in complete accordance with the earlier findings. The powder X-ray and neutron diffraction data confirm unambiguously that Mn and Cr are randomly (long range) distributed over the metal sub-lattice of an MnP type crystal structure (*Pnma* setting, $c>a>b$). The unit cell dimensions and positional parameters, as derived by Rietveld analyses of the powder neutron diffraction data, are listed in Table 1.

In line with the findings[6-9,13] for other $Mn_{1-t}T_tP$ phases, the positional parameters of $Mn_{1-t}Cr_tP$ (Table 1) remain constant within two calculated standard deviations for $0.00 \leqq t \leqq 0.40$ and $10 \leqq T \leqq 293$ K (*cf.* Ref. 8). The compositional dependence of the unit cell dimensions of $Mn_{1-t}Cr_tP$ for $0.00 \leqq t \leqq 0.40$ at 10 and 293 K is shown in Fig. 1. The agreement between the X-ray and neutron diffraction data is seen to be good, as is also the case with respect to the room temperature data in Ref. 10. In conformity with the other $Mn_{1-t}T_tP$

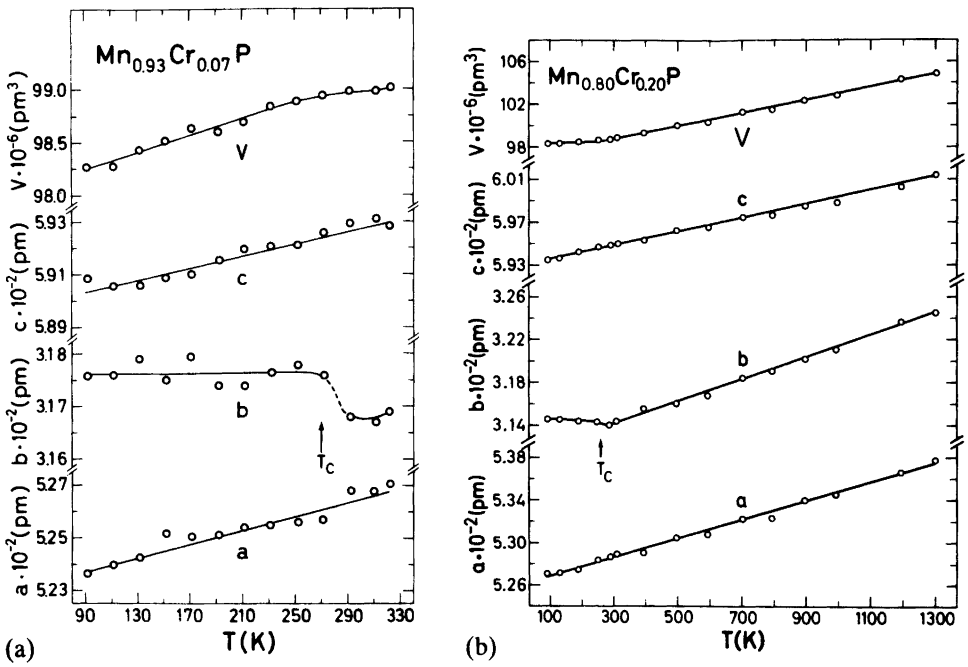

Fig. 2. Unit cell dimensions *versus* temperature for (a) $Mn_{0.93}Cr_{0.07}P$ and (b) $Mn_{0.80}Cr_{0.20}P$. *Calculated* error limits do not exceed the size of symbol. (1 Å=10^2 pm.) T_C refers to the P⇄F transition temperature observed by magnetization measurements.[2]

phases,[6-9,13] the *b* axis of $Mn_{1-t}Cr_tP$ is expanded between 293 and 10 K for part of the compositional range studied. However, for the $Mn_{1-t}Cr_tP$ phase (as opposed to the other $Mn_{1-t}T_tP$ phases) the contraction of *b* concerns only a part ($0.00 \leqq t \leqq \sim 0.25$ according to Fig. 1) of the stability range of the F phase ($0.00 \leqq t < \sim 0.5$). This deviation from the general pattern may be explained by the relatively low Curie temperatures (T_C) and ferromagnetic moments (μ_F) for $Mn_{1-t}Cr_tP$ with $\sim 0.3 < t < 0.5$, which reduce the effect of the magnetostriction.

The temperature variations of the unit cell dimensions of $Mn_{0.93}Cr_{0.07}P$ (90–310 K) and $Mn_{0.80}Cr_{0.20}P$ (90–1300 K) in Fig. 2 may serve as representative examples of the results obtained for various compositions of $Mn_{1-t}Cr_tP$. The P⇄F transition temperatures estimated from the kink points of the thermal expansion curves for *b* are consistently higher (20–50 K) than those derived by magnetic susceptibility, neutron diffraction and magnetization measurements [see (ii), (iii) and Ref. 2]. A systematic distinction and/or lesser sensitivity for the X-ray technique are/is not surprising, since this observes the combined effects of magnetostriction and thermal expansion/contraction. A comparison of Figs. 2a and b brings out that evaluation of the kink point on the thermal expansion curve for *b* is much easier when high temperature data are also included.

(ii) *Magnetic susceptibility.* The magnetic susceptibility data reported in Ref. 10 differ from those in Ref. 1 as well as from the results for other $Mn_{1-t}T_tP$ phases[6-9,13] in that the paramagnetic moment is constant for $0.00 \leqq t \leqq 0.40$. In order to resolve this divergence fresh magnetic susceptibility data were recorded for the present neutron diffraction samples, as well as for those examined in Ref. 10. The results show that there is no systematic distinction

between corresponding samples from the two sets of data. (Thus, our findings for $Mn_{1-t}Cr_tP$ and $Mn_{1-t}V_tP$ differ in this respect.) The present $\chi^{-1}(T)$ curves differ only slightly from those presented in Ref. 10. Nevertheless, there are some small, but significant distinctions which are brought out by the new data. Apart from a slight, almost unimportant calibration error, we believe that the mistakes which were made in Ref. 10 can be classified under "psychologically induced errors in measurements and/or interpretations", which refers to a process where certain facts are suppressed and others over-emphasized. In this manner, during the evaluation of the experimental results in Ref. 10, too much emphasis was put on an apparent full linearity and parallelism of the $\chi^{-1}(T)$ characteristics for $0.00 \leqq t \leqq 0.40$.

The only $\chi^{-1}(T)$ curves which are strictly linear over the entire range $\theta(\approx T_C) < T < 1000$ K [*viz.* fulfil *one* Curie-Weiss law relationship; $\chi^{-1} = C^{-1}(T-\theta)$] are those for $t < 0.20$. The curves for $0.20 \leqq t \leqq 0.40$ are better approximated by two such relationships, of which the data derived from the "high temperature Curie-Weiss regions" most likely have no simple physical interpretation. Paramagnetic moment ($\mu_{eff} = \sqrt{8C_{mol}}$) and Weiss constant ($\theta$) as derived from the Curie-Weiss regions and averaged over the three sets of data for $0.05 \leqq t \leqq 0.40$ (*vide supra*), are listed in Table 2, together with the corresponding number of unpaired spins ($2S$) according to the "spin only" approximation [$\mu_{eff} = g\sqrt{S(S+1)}$ with $g=2$]. Only the data estimated from the "low temperature Curie-Weiss regions" are considered below.

The θ values for $Mn_{1-t}Cr_tP$ (Table 2 or Refs. 1,10 which are in good mutual agreement in this respect) are consistently somewhat larger (10–30 K) than the corresponding T_C values

Table 2. Weiss constant (θ), paramagnetic moment (μ_{eff}) and number of unpaired spins ($2S$) for $Mn_{1-t}Cr_tP$ with $0.05 \leqq t \leqq 0.40$.

t	θ (K)	μ_{eff} (μ_B per Mn, Cr)	$2S$ (per Mn, Cr)	Range (K)
0.05	300±10	2.50±0.05	1.70±0.04	300–1000
0.10	285±10	2.45±0.05	1.65±0.04	285–1000
0.20	260±10	2.25±0.08	1.46±0.07	260–600
	210±15	2.45±0.15	1.65±0.13	600–1000
0.30	215±10	2.15±0.10	1.37±0.08	215–500
	160±15	2.45±0.15	1.65±0.13	500–1000
0.40	145±10	2.05±0.15	1.28±0.13	145–450
	70±15	2.50±0.10	1.70±0.08	450–1000

Table 3. Ferromagnetic parameters for $Mn_{1-t}Cr_tP$. The direction of the magnetic moment is parallel to *b*.

t	T (K)	μ_F (μ_B)	T_C (K)	T_S (K)
0.00	60	1.43(3)	292±4	53±3
0.05	60	1.46(5)	278±4	53±3[a]
0.10	60	1.41(6)	272±4	52±3[a]
0.20	60	1.33(7)	262±4	
	10	1.35(5)		
0.30	10	1.18(7)	189±8	
0.40	10	0.93(10)	142±10	

[a] Conversion to magnetic two phase (F and H_c).

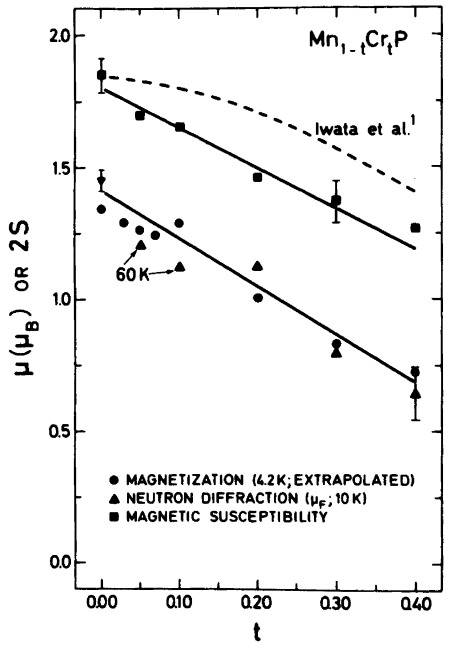

Fig. 3. Extrapolated magnetization moments (Ref. 2), neutron diffraction moments (μ_F) and paramagnetic ("spin only") $2S$ values *versus* the compositional parameter t. Legends to symbols are given on the illustration. Bars represent estimated or calculated errors.

derived by neutron diffraction and/or magnetization measurements. The relation between $2S$ and the magnetic moments obtained by neutron diffraction and magnetization measurements [see (iii) and Ref. 2] is shown in Fig. 3. The illustration demonstrates good conformity between the extrapolated magnetization moments and the ferromagnetic moments (μ_F). The paramagnetic $2S$ values are considerably higher than the ordered moments, *cf.* Refs. 6–9,13. The $2S$ *versus* t relationship derived from the data of Iwata *et al.*[1] falls above the present results and exhibits a somewhat non-linear behaviour. These distinctions may reflect differences in the sample preparations (*cf.* Ref. 2). A more detailed discussion of these findings will be given in relation to the corresponding data for all $Mn_{1-t}T_tP$ phases.

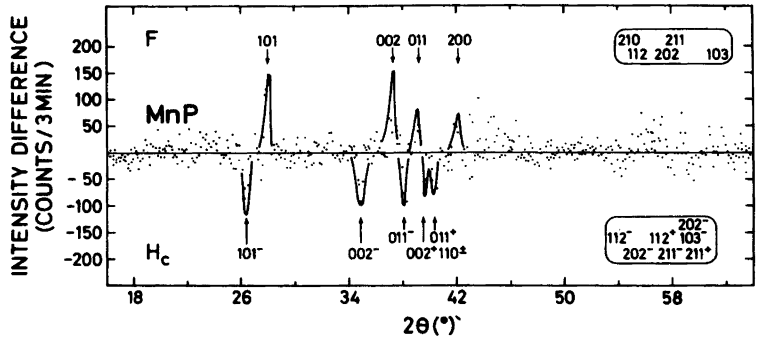

Fig. 4. Difference diagram between neutron diffraction patterns of MnP at 60 and 10 K. H_c and F refer to c axis helical and ferromagnetic states, respectively. Peak position and indexing are indicated on the illustration.

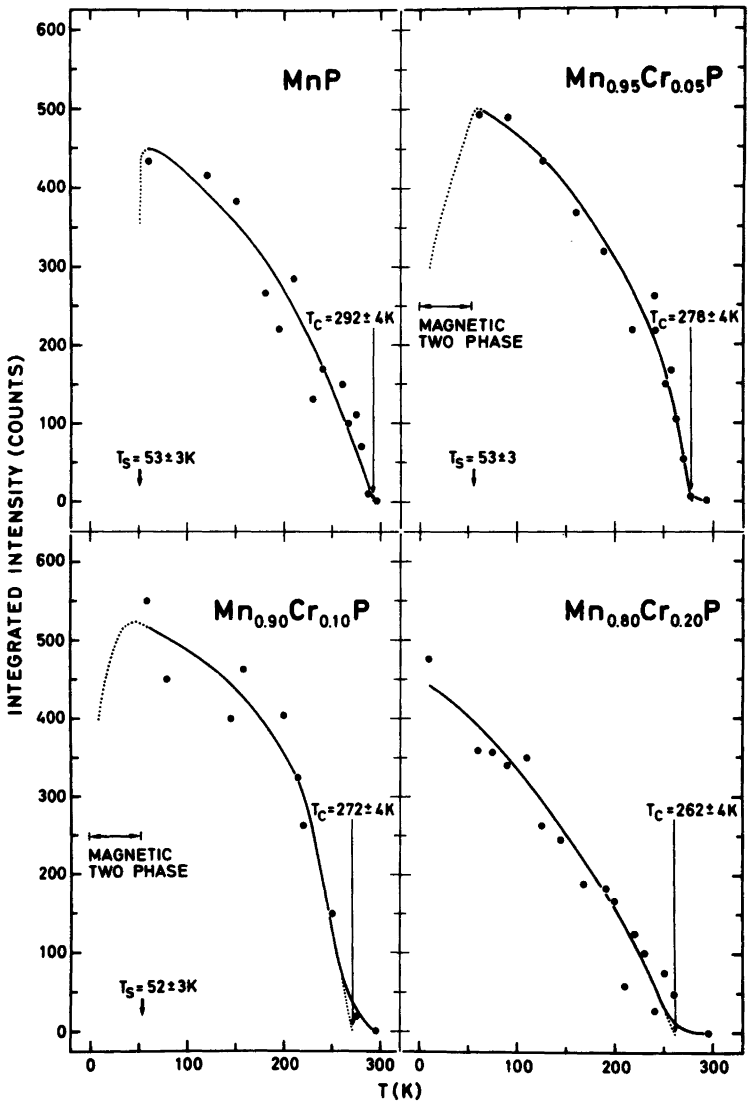

Fig. 5. Integrated intensity of ferromagnetic 202 *versus* temperature for MnP, $Mn_{0.95}Cr_{0.05}P$, $Mn_{0.90}Cr_{0.10}P$ and $Mn_{0.80}Cr_{0.20}P$. P⇄F and F to H_c transition temperatures (T_C and T_S, respectively) are indicated.

(iii) *Magnetic phase diagram and structures.* The present neutron diffraction results show that $Mn_{1-t}Cr_tP$ with $0.00 \leqq t \leqq 0.40$ undergoes a second (or higher) order P⇄F phase transition. Data for T_C and μ_F (direction of moments parallel to *b* ; *cf.* Refs. 3,6–9,13) are listed in Table 3. These findings are fully compatible with the magnetic phase diagram and other results for $Mn_{1-t}Cr_tP$ disclosed in Ref. 2.

On turning to the H_c phase, the situation becomes different. The existence range of this phase is considerably more narrow ($0.00 \leqq t \leqq \sim 0.02$) than advocated in Ref. 2; and a magnetic two phase region ($\sim 0.02 < t < \sim 0.11$) separates the H_c and F phases. The extensions

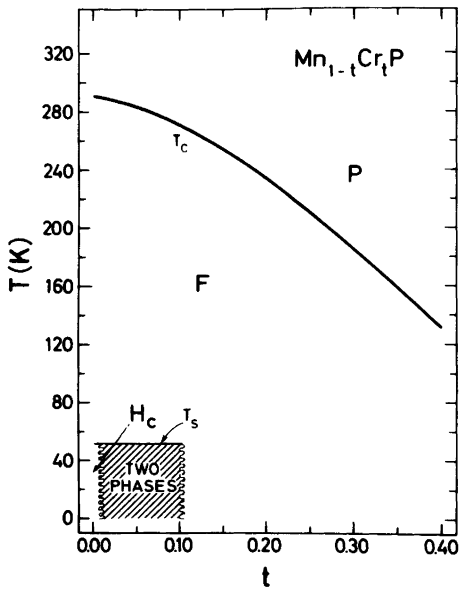

Fig. 6. Section of the magnetic phase diagram for $Mn_{1-t}Cr_tP$. Shaded area corresponds to magnetic two phase region. T_C is assessed from data in Refs. 1,2 and present results.

of the magnetic single and two phase regions are estimated from the samples with t=0.00, 0.05 and 0.10, which crystallographically all are single phase for 10<T<293 K, as judged from the present powder diffraction data. (It should be noted that the first order F to H_c transition in MnP itself involves only minor crystallographic changes.) A convenient way to detect temperature induced magnetic (or crystallographic) phase transitions is to make use of a difference diagram between the diffraction patterns obtained at two temperatures. The simple, neutron intensity, difference diagram for MnP (Fig. 4), which is crystallographic as well as magnetic single phase below 300 K (*cf.* Ref. 6), may serve as an example. Fig. 4 has been obtained by subtracting the (scaled) neutron diffraction intensities recorded for the H_c state at 10 K from that for the F state at 60 K. The clear-cut separation of the ferromagnetic peaks in the top half of Fig. 4 from the helimagnetic satellites in the bottom half indicates that the magnetic states of MnP are unmixed at these temperatures. The corresponding difference diagrams for $Mn_{0.95}Cr_{0.05}P$ and $Mn_{0.90}Cr_{0.10}P$ support the occurrence of a mixture of the F and H_c phases at 10 K.

The temperature variations of the ferromagnetic 202 reflection for MnP, $Mn_{0.95}Cr_{0.05}P$, $Mn_{0.90}Cr_{0.10}P$ and $Mn_{0.80}Cr_{0.20}P$ are shown in Fig. 5. This illustration also brings out the distinction between $Mn_{0.95}Cr_{0.05}P$ and $Mn_{0.90}Cr_{0.10}P$ on the the one hand and MnP (which converts completely to the H_c state below T_S) and $Mn_{0.80}Cr_{0.20}P$ (which remains in the F state dowm to 10 K) on the other. None of the curves in Fig. 5 fulfils a simple Brillouin type relationship.

A revised section of the magnetic phase diagram for $Mn_{1-t}Cr_tP$ is given in Fig. 6. As compared with the corresponding diagram in Ref. 2 the P⇄F phase boundary (T_C) has been assessed according to the best judgement of all available data (Refs. 1,2 and present). The situation for the H_c phase has been outlined above. The magnetic phase diagram for $Mn_{1-t}Cr_tP$ (Fig. 6) shows marked similarities with that for $Mn_{1-t}Ni_tP$,[7] and differs in various respects from the $Mn_{1-t}T_tP$ phases with T=V,[8] Fe,[9] Co,[6] Mo,[13] and W.[13]

The narrow existence range of the H_c phase and the occurrence of the H_c and F two phase region provide a very reasonable explanation of the virtually concentration

independent behaviour of the helimagnetic parameters T_S, τ_c (spiral propagation vector) and $\phi_{1,2}$ (phase angle between the spirals through atoms 1 and 2, *cf.* Ref. 5) reported in Ref. 2. (T_S is listed in Table 3, $\tau_c/2\pi c^*$ changes from 0.116±0.002 for MnP to 0.112±0.002 at the phase border and $\phi_{1,2}$ similarly from 24±3 to 28±3°.) The value for the helimagnetic moment (μ_H) is more difficult to assess from the magnetic two phase samples, but we suggest tentatively μ_H=1.35±0.10 μ_B (10 K) at the H_c phase border.

REFERENCES

1. Iwata, N., Fujii, H. and Okamoto, T. *J. Phys. Soc. Jpn. 46* (1979) 778.
2. Fjellvåg, H., Kjekshus, A., Zięba, A. and Foner, S. *J. Phys. Chem. Solids 45* (1984) 709.
3. Felcher, G.P. *J. Appl. Phys. 37* (1966) 1056.
4. Forsyth, J.B., Pickart, S.J. and Brown, P.J. *Proc. Phys. Soc. 88* (1966) 333.
5. Fjellvåg, H. and Kjekshus, A. *Acta Chem. Scand. A 38* (1984) 1.
6. Fjellvåg, H. and Kjekshus, A. *Acta Chem. Scand. A 38* (1984) 563.
7. Fjellvåg, H. and Kjekshus, A. *Acta Chem. Scand. A 38* (1984) 719.
8. Fjellvåg, H. and Kjekshus, A. *Acta Chem. Scand. A 38* (1984) 703.
9. Fjellvåg, H., Kjekshus, A. and Andresen, A.F. *Acta Chem. Scand. A 38* (1984) 711.
10. Selte, K., Fjellvåg, H. and Kjekshus, A. *Acta Chem. Scand. A 33* (1979) 391.
11. Bacon, G. E. In Yelon, W. B., Ed.,*Neutron Diffraction Newsletter,* Columbia 1977.
12. Watson, R.E. and Freeman, A. *Acta Crystallogr. 14* (1961) 27.
13. Fjellvåg, H. and Kjekshus, A. *Acta Chem. Scand. A 39* (1985). *In press.*

Received June 27, 1984.